Using matrix product states to study the dynamical large deviations of kinetically constrained models

Mari Carmen Bañuls[1,2] and Juan P. Garrahan[3,4]

[1] *Max-Planck-Institut für Quantenoptik, Hans-Kopfermann-Str. 1, D-85748 Garching, Germany*
[2] *Munich Center for Quantum Science and Technology (MCQST), Schellingstr. 4, D-80799 München*
[3] *School of Physics and Astronomy, University of Nottingham, Nottingham, NG7 2RD, UK*
[4] *Centre for the Mathematics and Theoretical Physics of Quantum Non-Equilibrium Systems, University of Nottingham, Nottingham, NG7 2RD, UK*

(Dated: July 28, 2019)

Here we demonstrate that tensor network techniques — originally devised for the analysis of quantum many-body problems — are well suited for the detailed study of rare event statistics in kinetically constrained models (KCMs). As concrete examples we consider the Fredrickson-Andersen and East models, two paradigmatic KCMs relevant to the modelling of glasses. We show how variational matrix product states allow to numerically approximate — systematically and with high accuracy — the leading eigenstates of the tilted dynamical generators which encode the large deviation statistics of the dynamics. Via this approach we can study system sizes beyond what is possible with other methods, allowing us to characterise in detail the finite size scaling of the trajectory-space phase transition of these models, the behaviour of spectral gaps, and the spatial structure and "entanglement" properties of dynamical phases. We discuss the broader implications of our results.

Introduction.– Dynamics equipped with local kinetic constraints provides a general mechanism for slow cooperative relaxation [1–4]. Kinetically constrained models (KCMs) — of which the Fredrickson-Andersen (FA) [2] and East [3] facilitated spin models are the simplest exponents — give many insights into the nature of glass forming systems, in particular by showing that systems with simple thermodynamics can have rich, spatially fluctuating and slow dynamics [5]. (For reviews on the glass transition see [6–8], and on KCMs see [9–11].) Beyond glasses, classical KCMs (and related deterministic models [12–16]) are relevant to the problem of operator spreading in quantum systems [17–24] and to non-equilibrium dynamics of ensembles of Rydberg atoms [25–27], while quantum KCMs provide a template for complex non-equilibrium dynamics under unitary evolution in the absence of disorder [28–31].

To characterise dynamics it is natural to study ensembles of stochastic trajectories, just like one does in equilibrium statistical mechanics with ensembles of configurations. For long-times one can then apply the methods of dynamical large deviations (LDs) [32] to compute quantities that play the role of thermodynamic potentials for the dynamics. For the case of KCMs such "thermodynamics of trajectories" [33] reveals the existence of a first-order phase transition in the space of trajectories between *active* and *inactive* dynamical phases, indicative of a singular change in atypical dynamical fluctuations [34, 35]. Many other systems have been now shown to have similar LD transitions, see e.g. [36–45].

The standard way of accessing LD statistics of a dynamical observable is by computing its scaled cumulant generating function (SCGF) — see below for definitions — from the largest eigenvalue of an appropriate deformation, or *tilting*, of the generator of the dynamics [11, 32, 36]. Except for the handful of non-trivial cases in which it can be calculated exactly [16, 37], obtaining the SCGF by diagonalising the tilted generator is only possible for small system sizes. To access the LD behaviour for larger sizes one has to resort to numerical methods for sampling rare trajectories based on splitting/cloning, importance sampling or optimal control [38, 46–52].

Here we show how to use variational matrix product states (MPS) to compute numerically with high accuracy (and precise control on errors) the SCGFs and the leading eigenstates of tilted generators by exploiting their similarity to quantum Hamiltonians, for larger systems than those accessible with other methods. We study in detail the FA and East models, focusing on the finite size scaling of their active-inactive phase transitions and the spatial structure of the dynamical phases. While in certain special cases MPS can be used to obtain exact LD statistics, such as in simple exclusion processes [53–57], hard core brownian particles [58], and certain cellular automata [16], the systematic application of numerical MPS methods to stochastic lattice systems has been limited [59]. Our results for KCMs — together with the recent ones [60] for simple exclusion processes — show the potential of numerical tensor network methods for the detailed study of fluctuations in stochastic dynamics.

FA and East models.– The FA [2] and East [3] models are defined in terms of binary variables, $\{n_i = 0, 1\}_{i=1}^{N}$, on the sites of a one dimensional lattice of size N, with single-spin flip dynamics subject to a kinetic constraint such that a spin can flip up (with rate c) or down (with rate $1 - c$) *only* if either nearest neighbour is in the up state (FA model) or *only* if the leftmost nearest neighbour is in the up state (East model). The generators for the

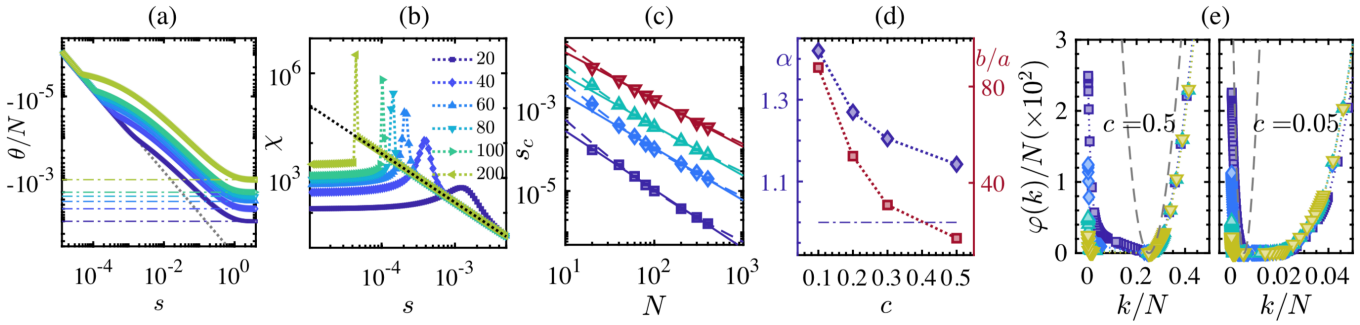

FIG. 1: **Finite size scaling of trajectory transition in the East model.** (a) SCGF $\theta(s)/N$ as a function of s at $c = 0.2$ for system sizes $N = 20$ to 200, showing the (extrapolated) crossing of the first two eigenvalues of $-H_s$. The dotted line corresponds to linear response, and the dot-dashed lines to the asymptotic values $\theta(s \to \infty) = -c$. (b) Dynamical susceptibilities, $\chi(s) = \theta''(s)$, exhibit a peak at $s_c(N)$ that gets sharper with N. For $s > s_c(N)$ we find an almost universal behavior $\chi \propto s^{-\gamma}$ with $\gamma \approx 1.4$. (c) $s_c(N)$ as a function of N for $N \in [20, 400]$ and various equilibrium concentrations c. The data is compatible with $\lim_{N\to\infty} s_c(N) \to 0$, but s_c appears to scale as $s_c(N) \propto N^{-\alpha}$ with $\alpha > 1$ (full lines are power-law fits; for comparison we also show fits to $a/N + b/N^2$, dashed). (d) The scaling exponents α (blue diamonds) and fitting parameters b/a (red squares) as a function of c. The departure from $1/N$ scaling (dotted-dashed) appears to be more pronounced the lower the c is. (e) Rate functions $\varphi(k)$ for $N \in [20, 200]$ at $c = 0.5$ (left) and $c = 0.05$ (right). Dashed lines correspond to Poisson distributions with average $\langle k \rangle = -\theta'(0)/N$. For the analogous results for the FA model see [61].

corresponding continuous time Markov chains are [9–11]

$$W^{\mathrm{FA,East}} = \sum_i \mathcal{C}_i^{\mathrm{FA,East}} \left[c\sigma_i^+ + (1-c)\sigma_i^- - c(1-n_i) - (1-c)n_i \right], \quad (1)$$

where $\sigma_i^\pm$ flips the site i up/down, and $\mathcal{C}_i^{\mathrm{FA}} = n_{i-1} + n_{i+1}$ or $\mathcal{C}_i^{\mathrm{East}} = n_{i-1}$ are the kinetic constraints for the FA and East models. The master equation is $\partial_t |P\rangle = W|P\rangle$, where $|P\rangle$ is the probability vector over configurations.

We consider *open boundary conditions*, which corresponds to setting $n_0 = n_{N+1} = 0$ in Eq. (1). This is computationally convenient for the MPS method we use and does not affect the physics we study (see discussion in [61]). Due to the kinetic constraints configuration space can be disconnected, and we consider the dynamics within the largest ergodic component: the set of all configurations with at least one up site for the FA, and all the configurations with fixed $n_1 = 1$ for the East model.

The above dynamics has stationary distribution $|P_{\mathrm{eq}}\rangle$ given by a projection of the product state $|c\rangle^{\otimes N}$, where $|c\rangle = (1-c)|0\rangle + c|1\rangle$, into the relevant ergodic component,

$$|P_{\mathrm{eq}}^{\mathrm{FA}}\rangle = [|c\rangle^{\otimes N} - (1-c)^N |0\rangle^{\otimes N}]/[1-(1-c)^N], \quad (2)$$

$$|P_{\mathrm{eq}}^{\mathrm{East}}\rangle = |1\rangle \otimes |c\rangle^{\otimes N-1}, \quad (3)$$

corresponding to the equilibrium distribution with energy $E = \sum_i n_i$ at inverse temperature $\ln(1-c)/c$.

Dynamical LDs and tilted generators.– As trajectory observable we consider the *dynamical activity* [34, 36, 62, 63], given by the total number of configuration changes $K(\omega_t)$ (i.e., number of spin flips) in a trajectory ω_t of time extent t. For large t, its probabilityobeys a LD principle, $P_t(K) = \langle \delta[K(\omega_t) - K] \rangle \approx e^{-t\varphi(K/t)}$, where $\varphi(x)$ is the LD rate function [32]. The corresponding moment generating function $Z_T(s) = \langle e^{-sK(\omega_t)} \rangle$ also obeys a LD principle, $Z_T(s) \approx e^{t\theta(s)}$, where $\theta(s)$ is the *scaled cumulant generating function* (SCGF), whose derivatives at $s = 0$ give the cumulants of K (scaled by t) [32]. The LD functions are connected by a Legendre transform, $\theta(s) = -\min_k [sk + \varphi(k)]$ [32] and play the role of thermodynamic potentials for trajectories.

The SCGF can be obtained from the largest eigenvalue of a tilted generator, W_s [32]. For the case of the dynamical activity, the tilt corresponds to multiplying the off-diagonal terms of W by a factor e^{-s} [34, 36]. Since the dynamics obeys detailed balance, the generators can be made Hermitian by a similarity transformation which is independent of s [35]. That is, if we define $H_s = -Q^{-1} W_s Q$, where Q is a diagonal matrix with elements $\langle \mathbf{n}|Q|\mathbf{n}\rangle = (1-c)^{N/2}[c/(1-c)]^{\sum_i n_i/2}$ in the configuration basis $\{|\mathbf{n}\rangle\}$, we get

$$H_s^{\mathrm{FA,East}} = -\sum_i \mathcal{C}_i^{\mathrm{FA,East}} \times \left[e^{-s}\sqrt{c(1-c)}\sigma_i^x - c(1-n_i) - (1-c)n_i \right]. \quad (4)$$

The SCGF therefore corresponds to (minus) the ground state energy of H_s, $\theta(s) = -E_{\mathrm{GS}}(s)$.

The relation between the ground state $|\Phi_{s0}\rangle$ of the tilted Hamiltonian, $H_s|\Phi_{s0}\rangle = E_{\mathrm{GS}}(s)|\Phi_{s0}\rangle$, and the left $\langle L_s|$ and right $|R_s\rangle$ leading eigenvectors of the tilted gen-

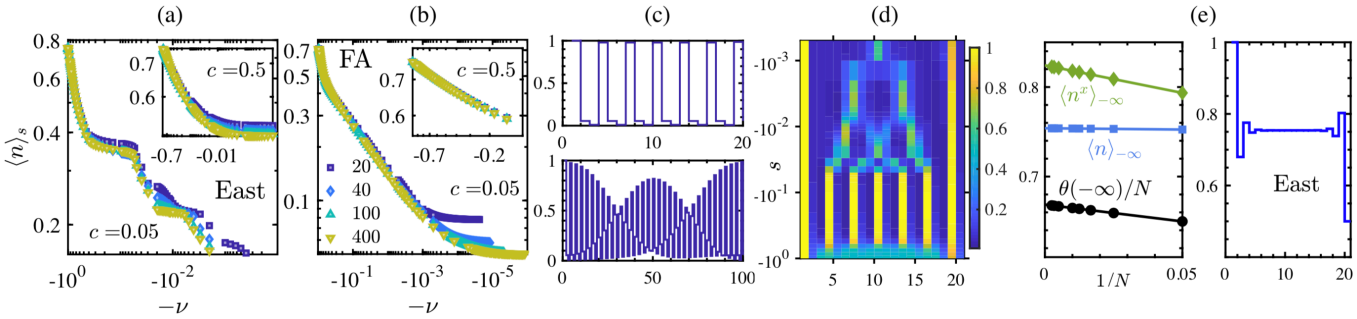

FIG. 2: **Structure of active phase.** (a) Mean density $\langle n\rangle_s$ for $s<0$ in the East model for $c=0.05$ (shown as function of $-\nu=e^s-1$). The plateau structure of the density is evident as compared to $c=0.5$ in the inset. (b) Same for the FA model, where the plateaus are absent. (c) Density profile of the ground state of H_s at $\nu=0.081$ ($s=-0.0845$) for the East model at $c=0.05$ for sizes $N=20$ (top) and 100 (bottom). (d) Density profiles across the active phase of the East model for $N=20$. (e) Extreme limit of the active phase, $s\to-\infty$, in the East model. On the left we show the rescaled $\tilde{\theta}(s=-\infty)/N:=e^s\theta(s=-\infty)/[N\sqrt{c(1-c)}]$ (black circles), $\langle n\rangle_{s=-\infty}$ (blue squares) and $\langle n^x\rangle_{s=-\infty}$ (green diamonds) for $N\in[20,400]$. The lines are fits to $a/N+b$ to extract the values in the thermodynamic limit: $\lim_{N\to\infty}\theta(s=-\infty)/N, \langle n^x\rangle_{s=-\infty}, \langle n\rangle_{s=-\infty}=0.67, 0.82, 0.75$. The right panels shows that the density profile at $s=-\infty$ is uniform, up to boundaries.

erator, $W_s|R_s\rangle=\theta(s)|R_s\rangle$, $\langle L_s|W_s=\langle L_s|\theta(s)$, is

$$|\Phi_{s0}\rangle=\sum_{\mathbf{n}}\sqrt{l_{\mathbf{n}}(s)r_{\mathbf{n}}(s)}\,|\mathbf{n}\rangle \tag{5}$$

where $l_{\mathbf{n}}(s)=\langle L_s|\mathbf{n}\rangle$ and $r_{\mathbf{n}}(s)=\langle\mathbf{n}|R_s\rangle$. The aim now is to compute $E_{\rm GS}(s)$ and $|\Phi_{s0}\rangle$ for Eq. (4).

Variational MPS method.– For a lattice of N d-dimensional quantum systems, a MPS [64] is a vector $|\Psi\rangle=\sum_{i_1,\dots i_N=1}^{d}\mathrm{tr}\left(A_1^{i_1}A_2^{i_2}\dots A_N^{i_N}\right)|i_1 i_2\dots i_N\rangle$, where i_k labels a local basis of the $k-$th subsystem, and each A_k is a rank-3 tensor of dimensions $d\times D\times D$ [65]. Such a state is described by $O(dND^2)$ parameters. The *bond dimension* D limits the entanglement of the state: in an MPS of bond dimension D, for any subchain A, the *entanglement entropy* (defined as $S_{\rm E}=-\mathrm{Tr}_A\rho_A\log\rho_A$, where $\rho_A=\mathrm{Tr}_{N\setminus A}|\Psi\rangle\langle\Psi|$ [66]) is upper-bounded by $S_{\rm E}\le 2\log D$, independent of the subchain length. Namely, MPS satisfy an entanglement *area law* [67], and conform a hierarchy of increasingly entangled states, with $D=d^{N/2}$ sufficing to describe the whole Hilbert space.

Conversely, MPS can efficiently approximate states that satisfy an area law [68], such as ground states of gapped local Hamiltonians. They are the basis for numerical methods like the density matrix renormalization group algorithm [69] which can be seen as a variational minimization of energy over MPS [70–74], by sequentially optimizing a single tensor, while keeping the rest constant, and iteratively sweeping until convergence [75]. We apply this strategy to find MPS approximations to the ground state and first excitations of the Hamiltonians (4). In this case, $d=2$ and the basis is $\{|\mathbf{n}\rangle\}$. As we show below, MPS with $D\ll 2^N$ provide accurate approximations for systems sizes at an order of magnitude larger than those accessible by other methods [76].

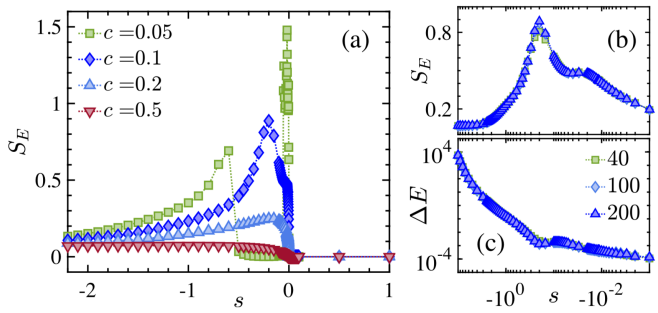

FIG. 3: **Entanglement.** (a) Half-chain entanglement entropy S_E of the ground state of H_s as a function of s for $c=0.5, 0.1, 0.05$ in the East model at $N=200$. (b) S_E for $s<0$ for $c=0.1$ at various sizes N. The peak is correlated with the change in shape of the spectral gap ΔE of H_s shown in (c).

Results. Finite size scaling of active-inactive trajectory transition.– The key property of KCMs like the FA and East is their first-order phase transition between an *active* phase for $s<0$ and *inactive* dynamical phase at $s>0$ [34, 35], manifested in a first-order singularity in the SCGF in the limit of $N\to\infty$. Like for all phase transitions, to characterise the transition and its associated fluctuations, it is necessary to understand how the singularity is approached as the system size increases. Theoretical and numerical considerations [77–79] suggest that for finite N the (rounded) transition occurs at $s_c(N)>0$ (i.e. typical dynamics, $s=0$, is perturbatively connected to the active phase), and $s_c(N)\to 0^+$ as $1/N$. These predictions can be tested with our MPS method.

Figure 1(a) shows (minus) the energy density $-E_{\rm GS}(s)/N=\theta(s)/N$ of the MPS solution as a function

of s for the East model (see [61] for the corresponding results for the FA model). The transition at $s_c(N)$ occurs where the two branches cross. The leftmost branch is linear in s and proportional to N, corresponding to the linear response for $s \gtrsim 0$ (grey dashed line). The rightmost branch is nonlinear, connecting the regime at $s \gtrsim 0$ to the asymptotic $\theta(\infty) = -c$.

The corresponding susceptibility $\chi_s = \theta''(s)/N$ shows a diverging peak at $s_c(N)$, see Fig. 1(b) [76]. From its peak we can estimate the location of $s_c(N)$. We find a departure from the expected $1/N$ scaling. Figure 1(c) shows that $s_c(N)$ can be fit to a power law, $s_c(N) \propto N^{-\alpha}$ with $\alpha > 1$ throughout. Figure 1(d) shows the dependence of the exponent α with c (blue symbols, left axis). The departure from $1/N$ in the fit becomes more pronounced with decreasing c. An alternative interpretation is that the discrepancy with $1/N$ scaling is due to subleading corrections in $1/N$. This possibility is tested in Fig. 1(c) (dashed lines). The dependence with c of the fitting parameters a and b is shown in Fig. 1(d) (red symbols, right axis). While both explanations appear equally plausible, the departure from $1/N$ in the data is evident, and demonstrates the power of the MPS for obtaining precise results in the vicinity of the phase transition.

The transition at s_c is associated with large fluctuations of the activity in the dynamics generated by Eq. (1), manifested in a non-Gaussian activity distribution. Figure 1(e) shows the LD rate function, $\varphi(K/t) = \lim_{t\to\infty} t^{-1} \log P_t(K)$, for different systems sizes. The broadening with N is as expected for a first order transition [34, 35]. For more details on the finite size scaling analysis including comparison with the predictions of Ref. [77] see [61].

Structure of active phase.– While both models have similar active-inactive transitions, their active phases differ. Figures 2(a,b) show the average density of excitations, $\langle n\rangle_s = N^{-1}\sum_{i=1}^{N}\langle\Phi_{s0}|n_i|\Phi_{s0}\rangle$, in the MPS that approximates the ground state of H_s for $s < 0$. In the East model and for small c, $\langle n\rangle_s$ shows a series of plateaus as s becomes more negative. These plateaus are absent in the FA model at the same c, Fig. 2(b), and also when the equilibrium concentration c is high, see insets to Figs. 2(a,b). These detailed results from our MPS method confirm the predictions of Ref. [80]

Figures 2(c,d) show the spatial structure of the active phase of the East model. In Fig. 2(c) we give the density profile at $s = -0.0845$ ($\nu = 0.081$) corresponding to the plateau in Fig. 2(a) with density $\langle n\rangle_s \approx 1/3$: the state is anticorrelated in space, with an occupied site followed by two nearly empty ones. This is evident in the $N = 20$ case, shown in the figure, while for $N = 100$ we also observe a longer ranged modulation of this pattern [76]. The spatial modulation is present throughout the $s < 0$ phase, as shown in Fig. 2(d). The spatial structure of the inactive state is absent in the FA model, see [61].

While the extreme inactive limit, $s \to \infty$, of the East model is very simple (since $|\Phi_{\infty 0}\rangle = |10\ldots0\rangle$), the extreme active limit, $s \to -\infty$, is highly non-trivial. In this limit we find that a MPS of $D \sim O(10)$ is enough to obtain a very precise approximation to the ground state over the whole range of sizes computed, $N \in [20, 400]$. We can then extrapolate to $N \to \infty$. We obtain, Fig. 2(e), for the limiting SCGF of the East model $\lim_{N\to\infty}\lim_{s\to-\infty} e^s\theta_{\rm E}(s)/[N\sqrt{c(1-c)}] \approx 0.6687$, with densities $\lim_{N\to\infty}\langle n\rangle_{-\infty} \approx 0.754$ and $\lim_{N\to\infty}\langle n^x\rangle_{-\infty} \approx 0.824$ (where n^x is the "transverse" magnetisation, $2n^x = 1-N^{-1}\sum_{i=1}^{N}\sigma_i^x$). The right panel of Fig. 2(e) shows that the spatial modulation at negative but finite s is absent at $s \to -\infty$ [81]. The FA model behaves in a similar manner in this limit, see [61].

Entanglement.– The states at $s \neq 0$ have spatial correlations absent in equilibrium ($s = 0$) and which varies with s. This can be quantified via their entanglement entropy, which together with other quantum information measures can capture changes in dynamical behaviour that might escape classical order parameters [82]. The entanglement entropy is easily computed for a state in MPS form. Figure 3(a) shows the half-chain S_E of the state $|\Phi_{s0}\rangle$ as a function of s in the East model at size $N = 200$. It is zero in the equilibrium state, cf. Eq. (3), and very small in the inactive phase, where the leading eigenvector is close to a product state of all sites empty in the bulk. For $s < 0$ it shows interesting structure, as expected from the spatial correlations of Fig. 2. In Fig. 3(b) we notice that the maximum of $S_{\rm E}$ does not seem to scale with system size. Thus, in the language of quantum many-body systems, the ground state fulfils an area law. This is also the case for other entropic quantities [76], which justifies the accuracy of the MPS approximation.

The peak in S_E nevertheless is sensitive to changes in the structure of the active phase. Fig. 3(c) shows the corresponding gap between $E_{\rm GS}(s)$ and the eigenvalue of the first excited state: its s dependence changes at a value of s located by the peak in S_E. (Note also that the gap is has no significant N dependence.) The maximum of the entropy depends on the value of c, and we find a larger peak for smaller values, corresponding to richer structure in the active phase, see Fig. 3(a) and [76].

Even if the entanglement is low throughout the phase diagram, cf. Fig. 3(a), this does not guarantee that the variational method will easily find an MPS approximation. In fact, we find that both for the region close to the phase transition at $s = 0$ and for the values of s where $S_{\rm E}$ shows a peak, cf. Fig. 3(a,b), the numerical convergence is slower than would have been expected. We believe this is a consequence of how the spectrum of the Hamiltonian changes when approaching these regimes [76].

Discussion.– As we have shown here, the MPS methods often employed in quantum many-body problems [74],

are also well suited for the study of the dynamical generators of classical stochastic systems [12–16, 53–60]. We focused on the LD statistics of KCMs such as the FA and East models, and showed how variational MPS approximations allow to efficiently access system sizes which are larger by an order of magnitude compared to previous studies, thus providing detailed information about the properties of the transitions in these models and the nature of the dynamical phases. Note also that in contrast to sampling methods such as cloning or TPS, our MPS approach provides an accurate estimate of the leading eigenvector, and thus of the full spatial statistics of the various dynamical phases.

We foresee many other applications of tensor networks in classical stochastic dynamics. Here we have focused on dynamics with detailed balance, and thus with generators similar to Hermitian operators, but efficient MPS algorithms also exist to find the "ground states" of non-Hermitian operators [**?**]. This suggest a natural extension to driven stochastic systems. Other applications include the study of dynamical transitions that are continuous rather than first-order, and the study of systems in dimension larger than one (for example via so-called PEPs [**?**]). More broadly, the crossover of ideas and techniques between quantum many-body and classical stochastics remains a fruitful area of investigation.

Acknowledgements – This work was supported by the Deutsche Forschungsgemeinschaft (DFG, German Research Foundation) under Germany's Excellence Strategy – EXC-2111 – 390814868, by EPSRC Grant No. EP/R04421X/1 and by the Leverhulme Trust Grant No. RPG-2018-181. We acknowledge the hospitality of the Kavli Institute for Theoretical Physics at the University of California, Santa Barbara, where this work was started, and support from the National Science Foundation under Grant No. NSF PHY-1748958.

[1] R. G. Palmer, D. L. Stein, E. Abrahams, and P. W. Anderson, Phys. Rev. Lett. **53**, 958 (1984).
[2] G. H. Fredrickson and H. C. Andersen, Phys. Rev. Lett. **53**, 1244 (1984).
[3] J. Jäckle and S. Eisinger, Z. fur Phys. B **84**, 115 (1991).
[4] W. Kob and H. C. Andersen, Phys. Rev. E **48**, 4364 (1993).
[5] J. P. Garrahan and D. Chandler, Phys. Rev. Lett. **89** (2002).
[6] K. Binder and W. Kob, *Glassy materials and disordered solids: An introduction to their statistical mechanics* (World Scientific, 2011).
[7] L. Berthier and G. Biroli, Rev. Mod. Phys. **83**, 587 (2011).
[8] G. Biroli and J. P. Garrahan, J. Chem. Phys. **138**, 12A301 (2013).
[9] F. Ritort and P. Sollich, Adv. Phys. **52**, 219 (2003).
[10] J. P. Garrahan, P. Sollich, and C. Toninelli, in *Dynamical Heterogeneities in Glasses, Colloids, and Granular Media*, International Series of Monographs on Physics, edited by L. Berthier, G. Biroli, J.-P. Bouchaud, L. Cipelletti, and W. van Saarloos (Oxford University Press, Oxford, UK, 2011).
[11] J. P. Garrahan, Physica A **504**, 130 (2018).
[12] T. Prosen and C. Mejía-Monasterio, J. Phys. A **49**, 185003 (2016).
[13] A. Inoue and S. Takesue, J. Phys. A **51**, 425001 (2018).
[14] T. Prosen and B. Buča, J. Phys. A **50**, 395002 (2017).
[15] K. Klobas, M. Medenjak, T. Prosen, and M. Vanicat, arXiv:1807.05000 (2018).
[16] B. Buča, J. P. Garrahan, T. Prosen, and M. Vanicat, arXiv:1901.00845 (2019).
[17] A. Nahum, J. Ruhman, S. Vijay, and J. Haah, Phys. Rev. X **7**, 031016 (2017).
[18] D. A. Rowlands and A. Lamacraft, Phys. Rev. B **98**, 195125 (2018).
[19] X. Chen and T. Zhou, arXiv:1808.09812 (2018).
[20] S. Gopalakrishnan, Phys. Rev. B **98**, 060302 (2018).
[21] M. Knap, Phys. Rev. B **98**, 184416 (2018).
[22] M. C. Tran, A. Y. Guo, Y. Su, J. R. Garrison, Z. Eldredge, M. Foss-Feig, A. M. Childs, and A. V. Gorshkov, arXiv:1808.05225 (2018).
[23] S. Gopalakrishnan, D. A. Huse, V. Khemani, and R. Vasseur, Phys. Rev. B **98**, 220303 (2018).
[24] V. Alba, J. Dubail, and M. Medenjak, arXiv:1901.04521 (2019).
[25] I. Lesanovsky and J. P. Garrahan, Phys. Rev. Lett. **111**, 215305 (2013).
[26] A. Urvoy, F. Ripka, I. Lesanovsky, D. Booth, J. P. Shaffer, T. Pfau, and R. Löw, Phys. Rev. Lett. **114**, 203002 (2015).
[27] M. M. Valado, C. Simonelli, M. D. Hoogerland, I. Lesanovsky, J. P. Garrahan, E. Arimondo, D. Ciampini, and O. Morsch, Phys. Rev. A **93**, 040701 (2016).
[28] M. van Horssen, E. Levi, and J. P. Garrahan, Phys. Rev. B **92**, 100305 (2015).
[29] A. Smith, J. Knolle, D. L. Kovrizhin, and R. Moessner, Phys. Rev. Lett. **118**, 266601 (2017).
[30] Z. Lan, M. van Horssen, S. Powell, and J. P. Garrahan, Phys. Rev. Lett. **121**, 040603 (2018).
[31] C. Turner, A. Michailidis, D. Abanin, M. Serbyn, and Z. Papić, Nature Phys. **14**, 745 (2018).
[32] H. Touchette, Phys. Rep. **478**, 1 (2009).
[33] M. Merolle, J. Garrahan, and D. Chandler, Proc. Natl. Acad. Sci. USA **102**, 10837 (2005).
[34] J. P. Garrahan, R. L. Jack, V. Lecomte, E. Pitard, K. van Duijvendijk, and F. van Wijland, Phys. Rev. Lett. **98**, 195702 (2007).
[35] J. P. Garrahan, R. L. Jack, V. Lecomte, E. Pitard, K. van Duijvendijk, and F. van Wijland, J. Phys. A **42**, 075007 (2009).
[36] V. Lecomte, C. Appert-Rolland, and F. van Wijland, J. Stat. Phys. **127**, 51 (2007).
[37] C. Appert-Rolland, B. Derrida, V. Lecomte, and F. van Wijland, Phys. Rev. E **78**, 021122 (2008).
[38] L. O. Hedges, R. L. Jack, J. P. Garrahan, and D. Chandler, Science **323**, 1309 (2009).
[39] T. Speck, A. Malins, and C. P. Royall, Phys. Rev. Lett. **109**, 195703 (2012).
[40] J. K. Weber, R. L. Jack, and V. S. Pande, J. Am. Chem.

Soc. **135**, 5501 (2013).
[41] C. P. Espigares, P. L. Garrido, and P. I. Hurtado, Phys. Rev. E **87**, 032115 (2013).
[42] R. L. Jack, I. R. Thompson, and P. Sollich, Phys. Rev. Lett. **114**, 060601 (2015).
[43] D. Karevski and G. M. Schütz, Phys. Rev. Lett. **118**, 030601 (2017).
[44] Y. Baek, Y. Kafri, and V. Lecomte, Phys. Rev. Lett. **118**, 030604 (2017).
[45] T. Oakes, S. Powell, C. Castelnovo, A. Lamacraft, and J. P. Garrahan, Phys. Rev. B **98**, 064302 (2018).
[46] C. Giardina, J. Kurchan, and L. Peliti, Phys. Rev. Lett. **96**, 120603 (2006).
[47] F. Cérou and A. Guyader, Stoch. Anal. Appl. **25**, 417 (2007).
[48] V. Lecomte and J. Tailleur, J. Stat. Mech. **2007**, P03004 (2007).
[49] T. Nemoto, F. Bouchet, R. L. Jack, and V. Lecomte, Phys. Rev. E **93**, 062123 (2016).
[50] U. Ray, G. K.-L. Chan, and D. T. Limmer, J. Chem. Phys. **148**, 124120 (2018).
[51] K. Klymko, P. L. Geissler, J. P. Garrahan, and S. Whitelam, Phys. Rev. E **97**, 032123 (2018).
[52] G. Ferré and H. Touchette, J. Stat. Phys. **172**, 1525 (2018).
[53] B. Derrida and J. L. Lebowitz, Phys. Rev. Lett. **80**, 209 (1998).
[54] J. de Gier and F. H. L. Essler, Phys. Rev. Lett. **107**, 010602 (2011).
[55] A. Lazarescu and K. Mallick, Journal of Physics A: Mathematical and Theoretical **44**, 315001 (2011).
[56] M. Gorissen, A. Lazarescu, K. Mallick, and C. Vanderzande, Phys. Rev. Lett. **109**, 170601 (2012).
[57] N. Crampé, E. Ragoucy, V. Rittenberg, and M. Vanicat, Phys. Rev. E **94**, 032102 (2016).
[58] A. Lapolla and A. Godec, New J. Phys. **20**, 113021 (2018).
[59] M. Gorissen, J. Hooyberghs, and C. Vanderzande, Phys. Rev. E **79**, 020101 (2009).
[60] P. Helms, U. Ray, and G. K.-L. Chan, arxiv:1904.07336 (2019).
[61] Supplemental Material.
[62] M. Baiesi, C. Maes, and B. Wynants, Phys. Rev. Lett. **103**, 010602 (2009).
[63] C. Maes, arXiv:1904.10485 (2019).
[64] D. Perez-Garcia, F. Verstraete, M. M. Wolf, and J. I. Cirac, Quantum Inf. Comput. **7**, 401 (2007).
[65] In the case of open boundary conditions, as used in this work, the first and last tensors reduce to rank-2 tensors of dimensions $d \times D$.
[66] M. A. Nielsen and I. L. Chuang, *Quantum Computation and Quantum Information: 10th Anniversary Edition*, 10th ed. (Cambridge University Press, New York, NY, USA, 2011).
[67] J. Eisert, M. Cramer, and M. B. Plenio, Rev. Mod. Phys. **82**, 277 (2010).
[68] Strictly speaking, the statement holds for states which fulfill an area law in Renyi entropies $S_\alpha = \log(\mathrm{tr}\rho^\alpha)/(1-\alpha)$ with $0 < \alpha < 1$ [83].
[69] S. R. White, Phys. Rev. Lett. **69**, 2863 (1992).
[70] G. Vidal, Phys. Rev. Lett. **91**, 147902 (2003).
[71] F. Verstraete, D. Porras, and J. I. Cirac, Phys. Rev. Lett. **93**, 227205 (2004).
[72] I. P. McCulloch, J. Stat. Mech. **2007**, P10014 (2007).
[73] F. Verstraete, V. Murg, and J. Cirac, Adv. Phys. **57**, 143 (2008).
[74] U. Schollwöck, Ann. Phys. **326**, 96 (2011).
[75] Notice that it is also possible to define MPS directly in the thermodynamic limit, and optimize them numerically with appropriate methods [73, 74].
[76] For details on the MPS numerics, their convergence, and for the comprehensive set of results for both the FA and East models, see Supplemental Material.
[77] T. Bodineau, V. Lecomte, and C. Toninelli, J. Stat. Phys. **147**, 1 (2012).
[78] T. Bodineau and C. Toninelli, Commun. Math. Phys. **311**, 357 (2012).
[79] T. Nemoto, R. L. Jack, and V. Lecomte, Phys. Rev. Lett. **118**, 115702 (2017).
[80] R. L. Jack and P. Sollich, J. Phys. A **47**, 015003 (2013).
[81] The GS in the limit $s \to -\infty$ seems to be gapped and with low entanglement ($D \sim 10$ provides a very good approximation [76]). The GS energy of the FA in this limit is almost exactly twice the one for East, and the overlap of their states is very high, suggesting they have similar GS, or rather the FA one is the superposition of that of the East and the reflected "West" model.
[82] C. Castelnovo, C. Chamon, and D. Sherrington, Phys. Rev. B **81**, 184303 (2010).
[83] N. Schuch, M. M. Wolf, F. Verstraete, and J. I. Cirac, Phys. Rev. Lett. **100**, 030504 (2008).